Maximum Power-Point Theory for Thermoelectric Harvesters

Xi Li, *Graduate Student Member, IEEE*, and Gabriel A. Rincón-Mora, *Fellow, IEEE*
School of Electrical and Computer Engineering, *Georgia Institute of Technology*, Atlanta, GA, U.S.A.
xli832@gatech.edu and rincon-mora@gatech.edu

***Abstract*—Thermoelectric generators (TEGs) are resistive dc sources that supply the most power when their resistance drops half the dc voltage. Not all this power reaches the load, however. The energy-harvesting circuit that draws and transfers this power loses some of it in the form of heat. These ohmic losses scale linearly and quadratically with current. From the perspective of the load, linear losses reduce the dc voltage of the source and quadratic losses raise the series resistance. This not only decreases the power delivered to the load but also shifts the maximum power point of the system. Neglecting this shift in maximum power point sacrifices 2.5% to 90% of the maximum achievable power when the added resistance is 10% to 50% of the thermoelectric resistance and the voltage loss is 5% to 23% of the thermoelectric voltage. This paper derives, models, and shows how the maximum power point of the thermoelectric harvester differs from that of the TEG and when that difference is significant.**

***Index Terms*— TE, MPP, P_{IN}, P_O, P_{LOSS}, Energy Harvester, Switched Inductor, DC voltage source, Source resistance, CMOS, MPP_{LOSS}, MPP model, DC-DC power supply, Boost, η_C.**

I. Thermoelectric-Powered Systems

Internet of Things (IoT) devices offer numerous benefits and functionalities. For instance, wireless sensors can monitor the production line by sensing chemicals [1]-[2]. However, these devices need to operate for months, and the use of large batteries can compromise their convenience. Recharging is also not a feasible option since most IoT devices are in hard-to-reach positions. Fortunately, thermoelectric generators (TEGs) provide solutions by generating voltage from thermal energy.

TEGs are low-power devices that can be modeled as a voltage source with a source resistance, as shown in Fig. 1. The voltage source generates v_T in the range of 40 mV to 400 mV, with ΔT ranging from 1-5 K. The source resistance R_T ranges from 1 Ω to 1.3 MΩ [3]. Due to the low v_T and large R_T, TEGs can only avail a limited amount of temperature-dependent available power, ranging from 0.3 nW to 3 mW, marked as P_{IN} in Fig. 1. Therefore, it is essential to collect energy at the maximum power points (MPPs) to obtain the most energy.

The MPPs of TEGs are dependent on the temperature difference (ΔT). Therefore, a maximum power point tracker (MPPT) is required for TEG power supplies. However, a harvester with MPPT has losses that consume power:

$$P_O = P_{IN} - P_{LOSS}, \tag{1}$$

where input power P_{IN} is the power before the harvester, and output power P_O represents the power available to loads as shown in Fig. 1. Hence, it is essential to maximize P_O, and the MPPs of P_O are of utmost importance.

This work is supported by Semiconductor Research Corporation Task No.2810.092 through UT Dallas' Texas Analog Center of Excellence (TxACE)

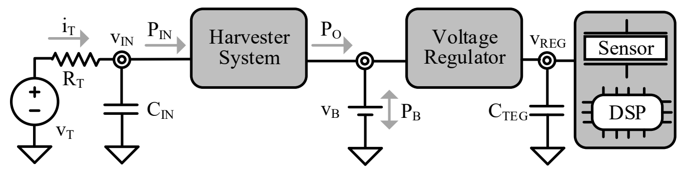

Fig. 1. Thermoelectric-powered system.

Several MPPT designs exist in the state of the art, with disagreement regarding which MPPs should be tracked. The majority of MPPTs stabilize the system at the MPPs of P_{IN} [4]-[29], while a minority of MPPT designs stabilize the system at the MPPs of P_O [30]-[33]. It remains unclear whether P_O reaches its maximum when the system maximizes P_{IN}, and systems in [4]-[29] could potentially harvest more energy. Therefore, this paper aims to explore the theory of MPPs of P_{IN} and P_O and provide a discussion on the maximum input power point (MIPP) and the maximum output power point (MOPP).

This paper is organized as follows: Section II discusses P_{IN} and its MPPs. Section III discusses P_O and its MPPs. Section IV explores the difference between MPPs of P_{IN} and P_O and discusses maximum power point loss. Section V discusses the design consideration. Section VI concludes the paper.

II. Maximum Input Power Point

P_{IN} is the power difference between the power from v_T and internal resistance loss P_{RT}:

$$P_{IN} = P_T - P_{RT} = v_T I_T - R_T {I_T}^2. \tag{2}$$

To determine the current for the maximum value of P_{IN}, the derivative of P_{IN} with respect to I_T is equated to zero:

$$\frac{\partial P_{IN}}{\partial I_T} = v_T - 2R_T I_T \equiv 0. \tag{3}$$

The value of I_T that satisfies this equation is denoted as $I_{T(IN)}'$, which represents the MIPP:

$$I_{T(IN)}' = \left(\frac{v_T}{2}\right)\left(\frac{1}{R_T}\right). \tag{4}$$

At $I_{T(IN)}'$, the maximum input power, $P_{IN(MIPP)}$, is obtained as:

$$P_{IN(MIPP)} = \left(\frac{v_T}{2}\right)^2\left(\frac{1}{R_T}\right). \tag{5}$$

This is the MPP as per the maximum power theorem, where the P_{IN} changes across I_T, and maximum P_{IN} is reached when I_T is half v_T over R_T, and the input voltage v_{IN} is half of v_T.

In Fig. 2, Load' represents the equivalent load seen by the TEGs, including the harvester, voltage regulator, and other components shown in Fig. 1. The maximum value of P_{IN} is obtained when Load' is equal to R_T.

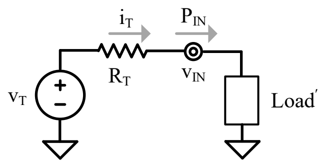

Fig. 2. Input power of TEG harvester system.

P_{RT} is associated with R_T. As shown in Fig. 3, the higher the P_{RT} is, the lower the power generated by TEG. Hence, TEGs with smaller values of R_T are preferred when v_T are the same.

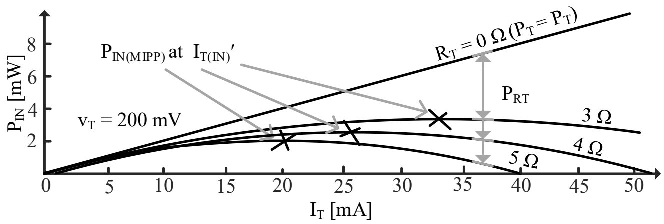

Fig. 3. Simulated P_{IN} changes with different R_T.

III. Maximum Output Power Point

Output power P_O refers to the power available to loads after P_{IN} flows through the harvester, as shown in Fig.4. Hence, the available power for loads is P_O, not P_{IN}. TEGs typically generate low v_T, which is often lower than the voltage requirements of loads, so the harvester in Fig. 4 must provide a boosting function to increase low v_T to v_B. Boosting can be achieved using either switched inductors or switched capacitors since only switched converters offer this function.

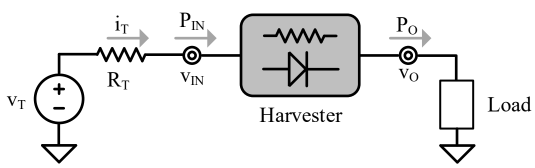

Fig. 4. Output power of TEG harvester system.

A. Losses

Switched converters generally have three types of losses. They always consume an ohmic loss P_R, which is proportional to the square of I_T:

$$P_R = R_H I_T^{\,2}, \tag{6}$$

where R_H is the equivalent resistance of the switched converter used as the harvester. P_R is proportional to I_T^2 as shown in Fig. 5. This type of loss is represented by a resistor in Fig. 4. Switched converters also have losses that are independent of I_T, such as the gate drive loss P_G which is produced when turning switches on and off:

$$P_G = v_{DD} q_G = v_{DD} C_{EQ} \Delta v_C, \tag{7}$$

where v_{DD} is the supply voltage of gate drivers, C_{EQ} denotes the equivalent gate capacitance of the switch, and Δv_C indicates the voltage change at the gate of the switch. To stabilize the system, a controller is required to manage switches. The power consumption of the controller is quiescent power P_Q:

$$P_Q = I_Q v_{DD}, \tag{8}$$

where i_Q is the total quiescent current of the controller. P_G and P_Q are losses that do not depend on I_T and are inherent to all switched converters.

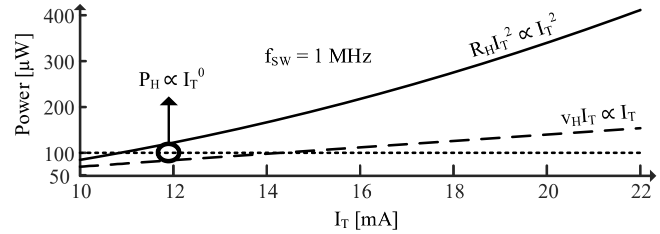

Fig. 5. Simulated losses dependencies on I_T.

In some systems, diode loss P_D may occur during operation due to a conducting diode:

$$P_D = v_D I_T \tag{9}$$

where v_D is the voltage across the conducting diode. P_D is linearly dependent on I_T, which is represented by a diode in Fig. 4. The total loss P_{LOSS} of a generalized harvester is:

$$P_{LOSS} = P_G + P_Q + P_D + P_R = P_H I_T^{\,0} + v_H I_T^{\,1} + R_H I_T^{\,2}, \tag{10}$$

where P_H is the power consumption of the harvester for losses independent of I_T. v_H is the equivalent voltage which denotes the losses with a constant voltage drops in the harvester.

B. Maximum Power

The power available to loads after the harvester system is denoted as P_O, as shown in Fig. 4. This P_O is what P_{LOSS} avails of P_{IN}. To determine the current for the maximum value of P_O, the derivative of P_O with respect to I_T is equated to zero:

$$\frac{\partial P_O}{\partial I_T} = \frac{\partial (P_{IN} - P_{LOSS})}{\partial I_T} = v_T - v_H - 2(R_T + R_H) I_T \equiv 0. \tag{11}$$

The value of I_T that satisfies this equation is denoted as $I_{T(O)}'$, which represents the MOPP:

$$I_{T(O)}' = \left(\frac{v_T - v_H}{2}\right)\left(\frac{1}{R_T + R_H}\right). \tag{12}$$

At $I_{T(O)}'$, the maximum output power, $P_{O(MOPP)}$, is obtained as:

$$P_{O(MOPP)} = \left(\frac{v_T - v_H}{2}\right)^2 \left(\frac{1}{R_T + R_H}\right) - P_H. \tag{13}$$

Similar to P_{IN}, P_O changes with I_T, and it reaches the maximum when I_T reaches $I_{T(O)}'$. When I_T is less than $I_{T(O)}'$, P_O rises as I_T increases. When I_T is greater than $I_{T(O)}'$, P_O falls as I_T increases, as shown in Fig. 6.

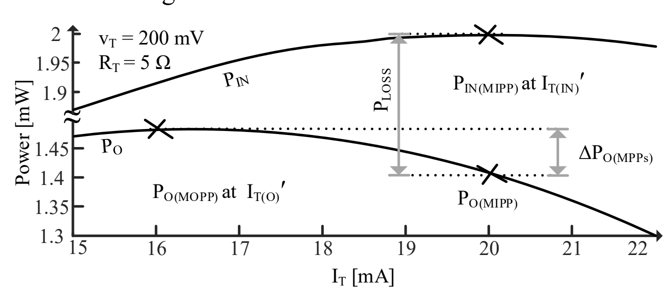

Fig. 6. Simulated P_O, P_{IN} with rising I_T.

IV. Maximum Power-Point Loss

A. MPP_{LOSS}

P_O reaches its MPP with a different current than P_{IN}, which means that when the system is stabilized to MIPP, P_O is smaller than its maximum. This is validated by observing P_O at $I_{T(IN)}'$:

$$P_{O(MIPP)} = P_{O(MOPP)} - \left(\frac{v_H}{2}\right)^2\left(\frac{1}{R_T}\right) - \frac{R_H}{R_T}\left[\left(\frac{v_T}{2}\right)^2\left(\frac{1}{R_T}\right) - \left(\frac{v_T - v_H}{2}\right)^2\left(\frac{1}{R_T+R_H}\right)\right]. \quad (14)$$

Comparing $P_{O(MOPP)}$ and $P_{O(MIPP)}$, the first term of $P_{O(MIPP)}$ is $P_{O(MOPP)}$, and the second term of the expression is negative. Inside the third term, the first half of the expression has a smaller denominator and a larger numerator compared to the second half, which means that the third term is also negative. Consequently, $P_{O(MIPP)}$ is less than $P_{O(MOPP)}$ as shown in Fig. 6.

If the system is stabilized to $I_{T(IN)}'$, it sacrifices P_O. To quantify this sacrifice due to different MPPs of P_{IN} and P_O, the maximum power points loss MPP_{LOSS} is defined as:

$$MPP_{LOSS} \equiv \left(\frac{\Delta P_{O(MPPs)}}{P_{O(MOPP)}}\right) = \left(\frac{P_{O(MOPP)} - P_{O(MIPP)}}{P_{O(MOPP)}}\right)$$
$$= \left(\frac{1 + \frac{R_H}{R_T}}{\left(\frac{v_H}{v_T}\right)^2 + 1 - \frac{2v_H}{v_T}}\right)\left[\left(\frac{v_H}{v_T}\right)^2 + \left(\frac{R_H}{R_T}\right)\right] - \frac{R_H}{R_T}, \quad (15)$$

where $\Delta P_{O(MPPs)}$ is the difference of P_O at MIPP and MOPP respectively as shown in Fig. 6. It is the fractional opportunity loss when the system is stabilized at MIPP instead of MOPP. The higher R_H and v_H, the higher P_O is sacrificed due to MIPP.

As shown in Fig. 7, when R_H is less than 10% of R_T and v_H is less than 5% of v_T, MPP_{LOSS} is less than 2.5%, making MPP_{LOSS} negligible. P_O at MIPP and MOPP exhibit similar values, allowing flexibility in choosing either MIPP or MOPP. However, when R_H is 50% of R_T and v_H is 23% of v_T, MPP_{LOSS} reaches about 91%, which means that P_O at MIPP is almost zero. Consequently, the system outputs almost no power even when operating at MIPP. In such cases, the system should operate at MOPP when MPP_{LOSS} exceeds the accepted range, such as 91%.

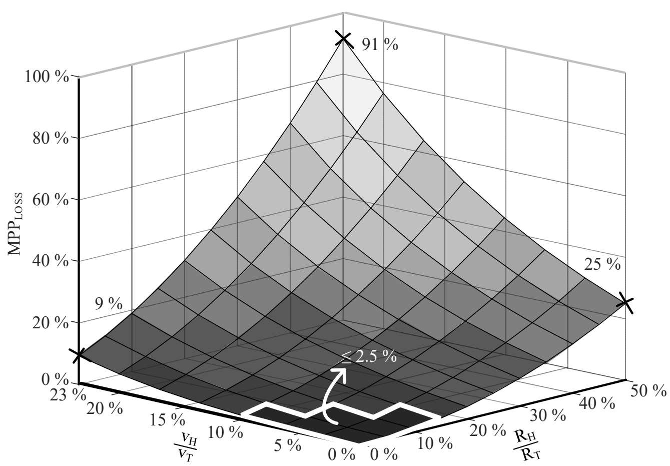

Fig. 7. MPP_{LOSS} with different R_H and v_H.

B. MPP Model

P_{IN} and P_O are related by P_{LOSS}, but $I_{T(IN)}'$ is distinct from $I_{T(O)}'$. Comparing $I_{T(O)}'$ and $I_{T(IN)}'$, the smaller numerator and larger denominator of $I_{T(O)}'$, resulting from R_H and v_H, make $I_{T(O)}'$ consistently smaller than $I_{T(IN)}'$:

$$I_{T(O)}' < I_{T(IN)}'. \quad (16)$$

Thus, in the system, P_O will attain the maximum power point first as I_T increases, followed by P_{IN} reaching its maximum power with a larger current level as shown in Fig. 6.

Fig. 8 shows an MPP model of an equivalent DC voltage source and series resistance, which simplifies the analysis of this inequality. In this model, R_H and v_H replace the harvester system as shown in the left circuit of Fig. 8. From the perspective of v_O, it has a new equivalent source voltage, which is the difference between v_T and v_H. The new equivalent source resistance is the series combination of R_T and R_H as shown in the circuit on the right in Fig. 8.

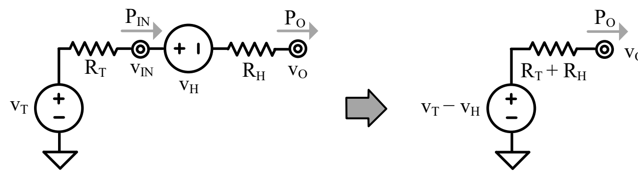

Fig. 8. MPP model of equivalent dc voltage source and series resistance

By utilizing this new equivalent MPP model, the same conclusions regarding $I_{T(O)}'$ and $I_{T(IN)}'$ can be drawn. For the new DC voltage source and series resistance, linear loss of the harvester reduces the new equivalent DC voltage source, while the quadratic loss increases the new equivalent series resistance.

C. Harvester-Charger Example

Figure 9 illustrates a boosting switched inductor, which serves as an example of a harvester-charger to validate the theory above. The circuit consists of a lithium-ion battery v_B with a voltage of 2.7 V, and a voltage source v_T of 200 mV with R_T of 5 Ω. v_{IN} delivers energy to v_B through inductor L_X, which has a series resistance R_L.

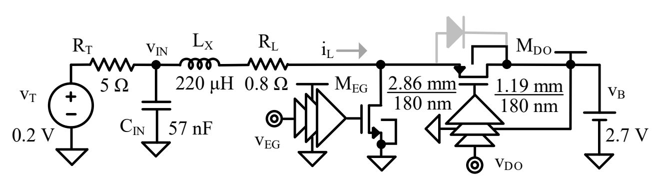

Fig. 9. Example of boosting harvester-charger.

The ground energize switch M_{EG} energizes L_X from v_{IN} to ground, while the output drain switch M_{DO} drains L_X from v_{IN} to v_B. These switches are implemented using MOSFET. This way, inductor current i_L draws P_{IN} from v_{IN} and outputs P_O to v_B. The circuit, as shown in Fig. 9, is simulated under continuous conduction mode (CCM).

In CCM, L_X conducts i_L continuously across conduction time t_{SW}, as shown in the simulated i_L waveform in Fig. 10 for a switching frequency of 1 MHz. When v_{IN} energizes L_X, i_L rises across energize time t_E. When v_B drains L_X, i_L decreases over drain time t_D. To prevent shorting v_B to ground, dead time t_{DT} is introduced during t_D. During t_{DT}, M_{EG} and M_{DO} are open, allowing v_B to drain L_X through the dead time diode in Fig. 9.

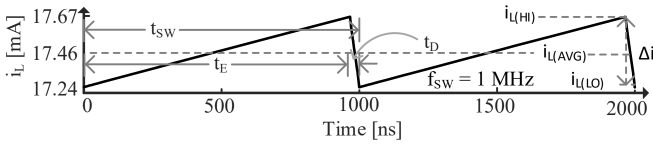

Fig. 10. Simulated inductor current i_L in continuous conduction mode.

When R_T is 5 Ω and v_T is 200 mV, the P_{IN} is shown in the bottom graph of Fig. 3, with a maximum value of 2 mW and MIPP of 20 mA. The losses of the switched inductor harvester are classified into quadratic loss, linear loss, and constant loss, and are plotted in Fig. 5. The P_O is shown in Fig. 6, with a maximum value of 1.48 mW and MOPP of 16 mA.

V. Harvester Design

A. Harvester Efficiency

The objective of a harvester is to obtain the highest possible P_O, which requires minimizing the harvester's losses. One common design approach for reducing losses is to maximize the harvester's efficiency η_C. η_C is the fraction of P_{IN} that reaches output as P_O:

$$\eta_C = \frac{P_O}{P_{IN}}. \tag{17}$$

In the SoA, as described in [16] and [21], some designs first determine the MIPP and then attempt to maximize the η_C of the harvester at MIPP to maximize the P_O. In other words, η_C, P_{IN}, and P_O reach the maximum at the same current level:

$$I_{T(C)}{}' = I_{T(O)}{}' = I_{T(IN)}{}', \tag{18}$$

where $I_{T(C)}{}'$ is the current level where maximum η_C is reached. However, this assertion is not always valid.

To determine the current for the maximum value of η_C, the derivative of η_C with respect to I_T is equated to zero:

$$\frac{\partial \eta_C}{\partial I_T} = \frac{P_{IN}\left(\frac{\partial P_O}{\partial I_T}\right) - P_O\left(\frac{\partial P_{IN}}{\partial I_T}\right)}{{P_{IN}}^2}$$
$$= \frac{P_H v_T - (R_T v_H + v_T R_H){I_T}^2 - 2P_H R_T I_T}{\left(v_T I_T - R_T {I_T}^2\right)^2} \equiv 0. \tag{19}$$

The value of I_T that satisfies this equation is denoted as $I_{T(C)}{}'$, which represents the maximum efficiency point:

$$I_{T(C)}{}' = \frac{\sqrt{P_H\left({v_T}^2 R_H + v_T R_T v_H + {R_T}^2 P_H\right)} - P_H R_T}{R_T v_H + v_T R_H}. \tag{20}$$

By plotting η_C, P_{IN}, and P_O as shown in Fig. 11, the MIPP, MOPP, and maximum efficiency point always follow:

$$I_{T(C)}{}' \le I_{T(O)}{}' \le I_{T(IN)}{}'. \tag{21}$$

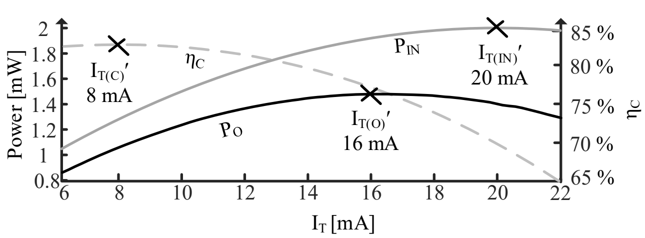

Fig. 11. η_C, $P_{IN(H)}$, and $P_{O(H)}$ changes with different I_T.

There is another way to illustrate this inequality. P_O is a η_C fraction of P_{IN}. As the product of two peaking functions, η_C and P_{IN}, P_O can only peak between the peaks of η_C and P_{IN}. As discussed in section III, the ohmic loss in the harvester shifts the MOPP away from MIPP. Therefore, for harvesters with ohmic loss, it is not possible to maximize η_C at MIPP, and maximizing η_C at MIPP is not a promising design direction.

B. MPP Theory

MIPP and MOPP represent different current levels due to the ohmic losses of the harvester and are equivalent when the harvester's R_H and v_H values are zero. Since MOPP is always different from MIPP, the harvester should operate at MOPP to maximize P_O. However, during the design process, there are additional factors to consider.

When R_H is less than 10% of R_T and v_H is less than 5% of v_T, the difference between MIPP and MOPP is less than 14%, and MPP_{LOSS} is less than 2.5%. As a result, $P_{O(MIPP)}$ is nearly identical to $P_{O(MOPP)}$. If MPP_{LOSS} is lower than the acceptable level of loss, MPPT can track either MIPP or MOPP. Designers then can choose which MPP to track based on chip area, controller power, and other factors.

The choice between MIPP and MOPP is also influenced by the characteristics of TEG. TEGs with higher R_T make it easier to restrict the harvester's R_H to less than 10% of RT than those with smaller R_T. Therefore, TEGs with higher R_T offer more design flexibility. Likewise, TEGs with higher v_T for the same ΔT provide greater flexibility for the same reason.

VI. Conclusions

This paper presents a theoretical analysis of the maximum power point (MPP) for both input power P_{IN} and output power P_O in thermoelectric-powered systems, validated by simulation. The study reveals that it's impossible to maximize P_{IN} and P_O simultaneously when the harvester experiences ohmic loss. Instead, the system would first maximize P_O with a lower source current and then maximize P_{IN} as the source current rises. The paper also introduces the concept of maximum power point loss, which results from operating the system at different MPPs. To conceptualize the impact of harvesters on MPPs, the paper proposes an MPP model. Furthermore, the analysis of the efficiency η_C and MPPs indicates that maximizing η_C at maximum P_{IN} does not necessarily result in maximum P_O. This paper demonstrates that TEGs with lower source resistance R_T offer higher P_O at the same temperature difference, while those with higher R_T provide greater design flexibility.

Acknowledgment

The authors would like to thank Dr. O. Lazaro, Dr. T. Chang, and Texas Instruments for their sponsorship and support.

References

[1] Y. Geng, Y. Ren, X. Wang, J. Li, L. Portilla, Y. Fang, and J. Zhao, "Highly sensitive and selective H2S sensors with ultra-low power consumption based on flexible printed carbon-nanotube-thin-film -transistors," *Sensors and Actuators B: Chemical*, vol. 360, pp. 131633–131644, 2022.

[2] J. Vincent and H.Lee, "Power Wearable Medical Device Components Via Thermoelectric Circuit Integration," *2019 IEEE Global Humanitarian Technology Conference (GHTC)*, Seattle, WA, USA, 2019, pp. 1-6.

[3] T. Chang and G. A. Rincón-Mora, "Design of switched-inductor charging regulator for resistive on-chip thermoelectric generators," *IEEE Trans. on Circuits and Syst. II*, vol. 69, no. 6, pp. 2872-2876, Jun. 2022.

[4] A. Montecucco and A. R. Knox, "Maximum Power Point Tracking Converter Based on the Open-Circuit Voltage Method for Thermoelectric Generators," *IEEE Trans. on Power Electronics*, vol. 30, no. 2, pp. 828-839, Feb. 2015.

[5] Z. Luo, L. Zeng, B. Lau, Y. Lian, and C.-H. Heng, "A Sub-10 mV Power Converter With Fully Integrated Self-Start, MPPT, and ZCS Control for Thermoelectric Energy Harvesting," *IEEE Trans. Circuits Syst. I: Regular Papers*, vol. 65, no. 5, pp. 1744-1757, May 2018.

[6] P. Cao, Y. Qian, P. Xue, D. Lu, J. He and Z. Hong, "A Bipolar-Input Thermoelectric Energy-Harvesting Interface With Boost/Flyback Hybrid Converter and On-Chip Cold Starter," *IEEE J. Solid-State Circuits*, vol. 54, no. 12, pp. 3362-3374, Dec. 2019.

[7] S. H. Wu, X. Liu, Q. Wan, Q. Kuai, Y. K. Teh, and P. K. Mok, "A 0.3-V Ultralow-Supply-Voltage Boost Converter for Thermoelectric Energy Harvesting With Time-Domain-Based MPPT," *IEEE Solid-State Circuits Letters*, vol. 4, pp. 100-103, 2021.

[8] N. Wang, J. N. Zhang, H. Ni, H. Z. Jia, and C. Ding, "Improved MPPT System Based on FTSMC for Thermoelectric Generator Array Under Dynamic Temperature and Impedance," *IEEE Trans. on Industrial Electronics*, vol. 69, no. 10, pp. 10715-10723, Oct. 2022.

[9] K.Yahya and O. Alomari, "A new maximum power point tracking algorithm based on power differentials method for thermoelectric generators," *International Journal of Energy Research*, vol. 45, issue 5, pp. 7476– 7486, 2021.

[10] B. Bijukumar, A. G. Raam, S. Ilango Ganesan, C. Nagamani, and M. J. Reddy, “MPPT algorithm for thermoelectric generators based on parabolic extrapolation,” *IET Generation, Transmission & Distribution*, vol. 13, no. 6, pp. 821–828, 2018.

[11] R.-Y. Kim, J.-S. Lai, B. York, and A. Koran, "Analysis and Design of Maximum Power Point Tracking Scheme for Thermoelectric Battery Energy Storage System," in IEEE Transactions on Industrial Electronics, vol. 56, no. 9, pp. 3709-3716, Sept. 2009.

[12] Y. S. Noh, J. I. Seo, H. S. Kim and S. G. Lee, "A Reconfigurable DC-DC Converter for Maximum Thermoelectric Energy Harvesting in a Battery-Powered Duty-Cycling Wireless Sensor Node," in ," *IEEE J. Solid-State Circuits*, vol. 57, no. 9, pp. 2719-2730, Sept. 2022,

[13] J. Tao, W. Mao, Z. Luo, L. Zeng and C. H. Heng, "A Fully Integrated Power Converter for Thermoelectric Energy Harvesting With 81% Peak Efficiency and 6.4-mV Minimum Input Voltage," *IEEE Trans. on Power Electronics*, vol. 37, no. 5, pp. 4968-4972, May 2022,

[14] Q. Kuai, H. Y. Leung, Q. Wan and P. K. T. Mok, "A High-Efficiency Dual-Polarity Thermoelectric Energy-Harvesting Interface Circuit With Cold Startup and Fast-Searching ZCD," *IEEE J. Solid-State Circuits*, vol. 57, no. 6, pp. 1899-1912, June 2022.

[15] J. Vega and J. Lezama, "Design and Implementation of a Thermoelectric Energy Harvester with MPPT Algorithms and Supercapacitor," *IEEE Latin America Transactions*, vol. 19, no. 01, pp. 163-170, January 2021.

[16] S. Bose, T. Anand and M. L. Johnston, "A 3.5-mV Input Single-Inductor Self-Starting Boost Converter With Loss-Aware MPPT for Efficient Autonomous Body-Heat Energy Harvesting," *IEEE J. Solid-State Circuits*, vol. 56, no. 6, pp. 1837-1848, June 2021.

[17] Rae-Young Kim and Jih-Sheng Lai, "Optimal design of adaptive maximum-power-point tracking algorithm for thermoelectric based battery energy storage system," 2008 *34th Annual Conference of IEEE Industrial Electronics*, Orlando, FL, USA, 2008, pp. 861-866.

[18] Z. Liu, Y. P. Hsu and M. M. Hella, "A Thermal/RF Hybrid Energy Harvesting System With Rectifying-Combination and Improved Fractional-OCV MPPT Method," *IEEE Trans. Circuits Syst. I: Regular Papers*, vol. 67, no. 10, pp. 3352-3363, Oct. 2020.

[19] P. Cao, Y. Qian, P. Xue, D. Lu, J. He and Z. Hong, "27.1 An 84% Peak Efficiency Bipolar-Input Boost/Flyback Hybrid Converter With MPPT and on-Chip Cold Starter for Thermoelectric Energy Harvesting," *2019 IEEE International Solid- State Circuits Conference (ISSCC)*, San Francisco, CA, USA, 2019, pp. 420-422.

[20] Q. Brogan *et al.*, "A Single Stage Boost Converter for Body Heat Energy Harvesting with Maximum Power Point Tracking and Output Voltage Regulation," *2019 IEEE International Symposium on Circuits and Systems (ISCAS)*, Sapporo, Japan, 2019, pp. 1-5.

[21] Q. Brogan and D. S. Ha, "A 3.5mV Input, 82% Peak Efficiency Boost Converter with Loss-Optimized MPPT and 50mV Integrated Cold-Start for Thermoelectric Energy Harvesting," *2019 IEEE Custom Integrated Circuits Conference (CICC)*, Austin, TX, USA, 2019, pp. 1-4.

[22] S. C. Chandrarathna and J. W. Lee, "A Dual-Stage Boost Converter Using Two- Dimensional Adaptive Input-Sampling MPPT for Thermoelectric Energy Harvesting," *IEEE Trans. Circuits Syst. I: Regular Papers*, vol. 66, no. 12, pp. 4888-4900, Dec. 2019.

[23] J. Pamod, S. Pumrin and B. Supmonchai, "An Input Capacitor-Less Boost Converter With Variation-Tolerant MPPT Circuit for Thermal Energy Harvesting*," 2018 15th International Conference on Electrical Engineering/Electronics, Computer, Telecommunications and Information Technology (ECTI-CON)*, Chiang Rai, Thailand, 2018, pp. 632-635.

[24] Y. Qian, H. Zhang, Y. Chen, Y. Qin, D. Lu and Z. Hong, "A SIDIDO DC–DC Converter With Dual-Mode and Programmable-Capacitor-Array MPPT Control for Thermoelectric Energy Harvesting," *IEEE Trans. Circuits Syst. II: Express Briefs*, vol. 64, no. 8, pp. 952-956, Aug. 2017

[25] X. Ge, X. Hu, Y. Qin and Z. Hong, "A single inductor tri-input dual-output buck-boost DC-DC converter with MPPT for multi-source energy harvesting," *2017 IEEE 12th International Conference on ASIC (ASICON)*, Guiyang, China, 2017, pp. 940-943.

[26] G. K. Thangam, T. Rakesh and S. E. Rajan, "Performance evaluation of non-isolated high step-up DC-DC converter for thermoelectric energy harvesting system using MPPT control techniques," *2016 International Conference on Circuit, Power and Computing Technologies (ICCPCT)*, Nagercoil, India, 2016, pp. 1-8.

[27] S. Nakayama, K. Kimura, Y. Kushino and H. Koizumi, "A simple MPPT control method for thermoelectric energy harvesting," 2015 IEEE Energy Conversion Congress and Exposition (ECCE). Montreal, QC, Canada, 2015, pp. 6455-6460.

[28] D. Merten, J. A. Singer, H. Fiedler, and S. Tappertzhofen, “Concept of an efficient self-startup voltage converter with dynamic maximum power point tracking for microscale thermoelectric generators,” *SN Applied Sciences*, vol. 4, no. 5, 2022.

[29] J. P. Im, S. W. Wang, S. T. Ryu and G. H. Cho, "A 40 mV Transformer-Reuse Self-Startup Boost Converter With MPPT Control for Thermoelectric Energy Harvesting," *IEEE J. Solid-State Circuits*, vol. 47, no. 12, pp. 3055-3067, Dec. 2012.

[30] N. Kanagaraj, H. Rezk, and M. R. Gomaa, “A Variable Fractional Order Fuzzy Logic Control Based MPPT Technique for Improving Energy Conversion Efficiency of Thermoelectric Power Generator,” *Energies*, vol. 13, no. 17, p. 4531, Sep. 2020.

[31] R. Malet, J. Oliver, R. Aragonés, R. Voces and C. Ferrer, "Power electronics for Waste Heat Recovery Unit with MPPT and Without Current Sensing," *IECON 2020 The 46th Annual Conference of the IEEE Industrial Electronics Society*, 2020, pp. 5197-5202.

[32] L. Jing, B. Song, Y. Zhu, B. Yang and H. Shu, "Grey Wolf Optimizer based MPPT Control of Centralized Thermoelectric Generator Applied in Thermal Power Stations," *2020 Asia Energy and Electrical Engineering Symposium (AEEES)*, pp. 127-132, 2020.

[33] H. O. Tabrizi, H. M. P. C. Jayaweera and A. Muhtaroğlu, "Fully Integrated Autonomous Interface With Maximum Power Point Tracking for Energy Harvesting TEGs With High Power Capacity," in *IEEE Trans. on Power Electronics*, vol. 35, no. 5, pp. 4905-4914, May 2020.